Two New One-Dimensional Compounds with End-to-End Dicyanamide as a Bridging Ligand: Syntheses and Structural Characterization of *trans*-$[Mn(4\text{-bzpy})_2(N(CN)_2)_2]_n$ and *cis*-$[Mn(Bpy)(N(CN)_2)_2]_n$, (4-bzpy = 4-benzoylpyridine; bpy = 2,2′-bipyridyl)

Albert Escuer,*,† Franz A. Mautner,‡ Núria Sanz,† and Ramon Vicente†

Departament de Química Inorgànica, Universitat de Barcelona, Diagonal 647, 08028 Barcelona, Spain, and Institut für Physikalische und Theoretische Chemie, Technische Universität Graz, A-8010 Graz, Austria

Received July 29, 1999

Two new one-dimensional compounds, *trans*-$[Mn(4\text{-bzpy})_2(N(CN)_2)_2]_n$ (**1**) and *cis*-$[Mn(bpy)(N(CN)_2)_2]_n$ (**2**), have been synthesized and studied from a magnetic point of view (4-bzpy = 4-benzoylpyridine; bpy = 2,2′-bipyridyl). The crystal structures of **1** and **2** have been solved. Compound **1** crystallizes in the monoclinic system, $P2_1/n$ group, $a = 6.374(2)$ Å, $b = 7.584(2)$ Å, $c = 26.766(5)$ Å, $\beta = 91.87°$, and $Z = 2$, whereas compound **2** crystallizes in the monoclinic system, $C2/c$ group, $a = 6.707(2)$ Å, $b = 17.188(5)$ Å, $c = 13.096(5)$ Å, $\beta = 90.54°$, and $Z = 4$. The two compounds consist of chains with double $\mu_{1,5}$-dicyanamide bridges between neighboring manganese(II) atoms. The weak antiferromagnetic coupling found for the two compounds ($J = -0.3$ cm^{-1} for **1** and -0.4 cm^{-1} for **2**) has been studied by MO analysis, and the superexchange pathway through the $\mu_{1,5}$-($NCNCN^-$) bridge has been compared with the shorter $\mu_{1,3}$-(NNN^-).

Introduction

Weak ferromagnets of general formula $[M(N(CN)_2)_2]$ with a 3-D rutile-type structure in which $N(CN)_2^-$ is the dicyanamide ligand (dca) have recently been the object of considerable attention because of the ability of the dca ligand to act as a molecular-based magnet precursor with several first-row transition ions such as Cu(II), Ni(II), Co(II), Mn(II), and Cr(II).[1] In addition to compounds of this kind, other high-dimensional systems based on the related tricyanomethanide ligand[2] or based on the mixing of different bridging ligands such as dicyanamide and pyrazine bridges[3] have been characterized and studied in the search for interesting magnetic properties. When the M/dca ratio is 1:2 and M is hexacoordinated, neutral three-dimensional compounds are formed as a consequence of the ability of the dca ligand to act as a tridentate ligand with the three nitrogen atoms (six coordination sites to six donor atoms, Chart 1A). If the coordination number is 4 instead of 6, the M/dca ratio of 1:2 allows the formation of a bidentate end-to-end $\mu_{1,5}$-dca ligand (four coordination sites to four donor atoms), as was found for $[Zn(dca)_2]$ [4] (Chart 1B). For hexacoordinated metallic centers with two coordination sites occupied by additional blocking ligands, the dca should also act as bidentate $\mu_{1,5}$-dca bridging ligand as was reported[3] for $[Mn(pyz)(dca)_2]$ (pyz = pyrazine) or may even act as a monodentate ligand through only one N-terminal atom for the $[ML_4(dca)_2]$ general formula (Chart 1C), as occurs in compounds such as $[Cu(phen)_2(dca)_2]$ (phen = 1,10-phenanthroline)[5] and $[Ni(4Meim)_4(dca)_2]$ (4Meim = 4-methylimidazole),[6] as a result of which the 1:2 ratio is maintained.

Chart 1

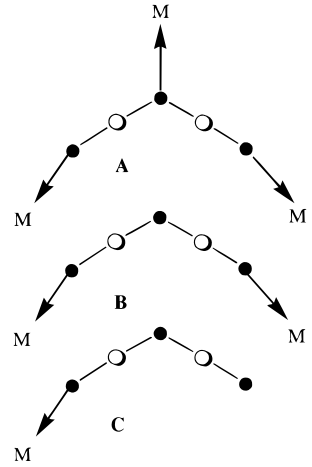

† Universitat de Barcelona.
‡ Technische Universität Graz.

(1) (a) Batten, S. R.; Jensen, P.; Moubaraki, B.; Murray, K. S.; Robson, R. *J. Chem. Soc., Chem. Commun.* **1998**, 439. (b) Kurmoo, M.; Kepert, C. J. *New J. Chem.* **1998**, *22*, 1515. (c) Manson, J. L.; Kmety, C. R.; Huang, Q. Z.; Lynn, J. W.; Bendele, G. M.; Pagola, S.; Stephens, P. W.; Liablesands, L. M.; Rheingold, A. L.; Epstein, A. J.; Miller, J. S. *Chem. Mater.* **1998**, *10*, 2552. (d) Jensen, P.; Batten, S. R.; Fallon, G. D.; Moubaraki, B.; Murray, K. S.; Price, D. J. *J. Chem. Soc., Chem. Commun.* **1999**, 177. (e) Manson, J. L.; Kmety, C. R.; Epstein, A. J.; Miller, J. S. *Inorg. Chem.* **1999**, *38*, 2552.

(2) (a) Hvastijova, M.; Kozisek, J.; Kohout, J.; Jager, L.; Fuess, H. *Transition Met. Chem.* **1995**, *20*, 276. (b) Manson, J. L.; Campana, C.; Miller, J. S. *J. Chem. Soc., Chem. Commun.* **1998**, 251. (c) Batten, S. R.; Hoskins, B. F.; Robson, R. *Inorg. Chem.* **1998**, *37*, 3432. (d) Hvastijova, M.; Kohout, J.; Kozisek, J.; Diaz, J. G.; Jager, L.; Mrozinski, J. *Z. Anorg. Allg. Chem.* **1998**, *624*, 349. (e) Triki, S.; Sala Pala, J.; Decoster, M.; Molinie, P.; Toupet, L. *Angew. Chem., Int. Ed. Engl.* **1999**, *38*, 113.

(3) Manson, J. L.; Incarvito, C. D.; Rheingold, A. L.; Miller, J. S. *J. Chem. Soc., Dalton Trans.* **1998**, 3705.

(4) Manson, J. L.; Lee, D. W.; Rheingold, A. L.; Miller, J. S. *Inorg. Chem.* **1998**, *37*, 5966.

(5) Potocnak, I.; Dunajjurco, M.; Miklos, D.; Kabesova, M.; Jager, L. *Acta Crystallogr. C* **1995**, *51*, 600.

(6) Kozisek, J.; Paulus, H.; Dankova, M.; Hvastijova, M. *Acta Crystallogr. C* **1996**, *52*, 3019.

10.1021/ic990905h CCC: $19.00
Published on Web 03/25/2000

The stoichiometric compound $[ML_2(dca)_2]$, in which L may be two monodentate ligands or one bidentate ligand (four free coordination sites remaining), should afford compounds with bidentate dca ligands as in the $[Zn(dca)_2]$ case. Following this strategy we have synthesized two new one-dimensional compounds in which M is manganese(II) and L_2 are two 4-benzoylpyridine or one 2,2′-bipyridyl, with the formula *trans*-$[Mn(4\text{-bzpy})_2(N(CN)_2)_2]_n$ (**1**) or *cis*-$[Mn(bpy)(N(CN)_2)_2]_n$ (**2**). In both cases the dca ligand was found to be coordinated in the expected $\mu_{1,5}$ bidentate mode. Susceptibility measurements indicate weak antiferromagnetic coupling with $J = -0.3$ and -0.4 cm^{-1}, respectively.

Compounds **1** and **2** have structures similar to those of the recently reported $\mu_{1,3}$-azide derivatives with formula $[Mn(L)_2(N_3)_2]$ (L = 2-hydroxypyridine or 3-ethylpyridine),[7] which also consist of chains with double end-to-end bridges. The most interesting difference lies in the moderately strong coupling (J ranging from -7 to -13 cm^{-1}) found for the azido derivatives. The different behavior as superexchange mediator between these two bridges, on the basis of the topology of the bridging ligands $\mu_{1,3}$-azido and $\mu_{1,5}$-dca, has been compared by means of MO calculations.

Experimental Section

Synthesis. The two compounds were prepared in a similar form. An amount of 5 mL of an aqueous solution of sodium dicyanamide (0.18 g, 2 mmol) was added dropwise to 50 mL of a methanolic solution of manganese nitrate hexahydrate (0.29 g, 1 mmol) and 2,2′bipyridyl (0.16 g, 1 mmol) or manganese nitrate hexahydrate (0.29 g, 1 mmol) and 4-benzoylpyridine (0.37 g, 2 mmol). The final clear yellow solution was left to evaporate. Good quality crystals were obtained after 2 weeks. The yield of the first crop was around 40% for both compounds. Analytical data for **1** found (calcd for $C_{28}H_{18}N_8MnO_2$): C, 61.2 (60.76); H, 3.3 (3.28); N, 20.9 (20.3). For **2** found (calcd for $C_{14}H_8N_8Mn$): C, 48.6 (48.95); H, 2.3 (2.34); N, 32.7 (32.63). For IR spectra, in addition to the characteristic bands of the corresponding pyridyl derivatives, a set of very intense bands of the dicyanamide groups appeared at 2308, 2233, and 2176 cm^{-1} for **1** and at 2302, 2232, 2206, and 2168 cm^{-1} for **2**.

Spectral and Magnetic Measurements. Infrared spectra (4000−400 cm^{-1}) were recorded from KBr pellets on a Nicolet 520 FTIR spectrophotometer. Magnetic measurements were carried out with a Quantum Design instrument with a SQUID detector in the temperature range 2−300 K under a 500 G field. Magnetization measurements were recorded up to 5 T of external magnetic field. Diamagnetic corrections were estimated using Pascal tables. EPR spectra were recorded with a Bruker ES200 spectrometer at X-band frequency equipped with an Oxford liquid-helium cryostat for variable temperature work.

Crystallographic Data Collection and Refinement of the Structures. $[Mn(4\text{-bzpy})_2(N(CN)_2)_2]_n$ (1) and $[Mn(bpy)(N(CN)_2)_2]_n$ (2). The X-ray single-crystal data for both compounds were collected on a modified STOE four-circle diffractometer. Crystal size: 0.55 mm × 0.40 mm × 0.22 mm for **1** and 0.42 mm × 0.18 mm × 0.18 mm for **2**. The crystallographic data, the conditions for the intensity data collection, and some features of the structure refinements are listed in Table 1. Graphite-monochromatized Mo Kα radiation ($\lambda = 0.710\ 69$ Å) and the ω-scan technique were used to collect the data sets. Accurate unit cell parameters were determined from automatic centering of 50 reflections ($10.2° < \theta < 16.4°$) for **1** and 47 reflections ($4.0° < \theta < 13.9°$) for **2** and refined by least-squares methods. A total of 2788 reflections (2278 independent reflections; $R_{int} = 0.0237$) were collected for **1** in the range $2.79° < \theta < 25.00°$ and 1595 reflections (1321 independent reflections; $R_{int} = 0.0269$) for **2** in the range $2.83° < \theta < 24.99$. Corrections were applied for Lorentz polarization effects and for absorption using the DIFABS[8] computer program (range of normalized transmission factors: 0.385−1.000 for **1** and 0.253−1.000 for **2**). The structures were solved by direct methods using the SHELXS-86[9] computer program and refined by full-matrix least-squares methods on F^2 for **2**, using the SHELXL-93[10] program incorporated in the SHELXTL/PC, version 5.03,[11] program library and the graphics program PLUTON.[12] All non-hydrogen atoms were refined anisotropically. The hydrogen atoms were located at calculated positions (C−H bond lengths of 0.930 Å), and their isotropic displacement factors were set at 1.2 times the value of the equivalent isotropic displacement parameter of the corresponding parent carbon atom. The final R indices were 0.0440 and 0.0452, respectively, for all observed reflections. Numbers of refined parameters were 178 (**1**) and 105 (**2**). Maximum and minimum peaks in the final difference Fourier syntheses were 0.417 and −0.386 e Å^{-3} for **1** and 0.235 and −0.172 e Å^{-3} for **2**. Significant bond parameters for **1** and **2** are given in Tables 2 and 3.

Table 1. Crystal Data and Structure Refinement for $[Mn(4\text{-bzpy})_2(N(CN)_2)_2]_n$ (**1**) and $[Mn(bpy)(N(CN)_2)_2]_n$ (**2**)

	1	**2**
chemical formula	$C_{28}H_{18}MnN_8O_2$	$C_{14}H_8MnN_8$
fw	553.44	343.22
space group	$P2_1/n$	$C2/c$
a, Å	6.374(2)	6.707(2)
b, Å	7.584(2)	17.188(5)
c, Å	26.766(5)	13.096(5)
β, deg	91.87(2)	90.54(2)
V, Å^3	1293.3(6)	1509.6(9)
Z	2	4
T, °C	25(2)	25(2)
λ(Mo Kα), Å	0.710 69	0.710 69
d_{calc}, g cm^{-3}	1.421	1.510
μ(Mo Kα), mm^{-1}	0.553	0.886
R^a	0.0440	0.0452
$R^2\omega^b$	0.1024[b]	0.0979[b]

[a] $R(F_o) = \sum(F_o - F_c)/\sum F_o$. [b] $R\omega(F_o)^2 = \{\sum[\omega((F_o)^2 - (F_c)^2)^2]/\sum[\omega((F_o)^2)^2]\}^{1/2}$.

Table 2. Selected Bond Lengths (Å) and Angles (deg) for $[Mn(4\text{-bzpy})_2(N(CN)_2)_2]_n$ (**1**)

Mn(1)−N(1)	2.212(2)	Mn(1)−N(1A)	2.212(2)
Mn(1)−N(3B)	2.221(3)	Mn(1)−N(3C)	2.221(3)
Mn(1)−N(4)	2.291(2)	Mn(1)−N(4A)	2.291(2)
N(1)−C(1)	1.130(3)	C(1)−N(2)	1.291(4)
N(2)−C(2)	1.295(4)	C(2)−N(3)	1.135(4)
N(1)−Mn(1)−N(1A)	180.0	N(1)−Mn(1)−N(3B)	86.49(9)
N(1A)−Mn(1)−N(3B)	93.51(9)	N(1)−Mn(1)−N(3C)	93.51(9)
N(1A)−Mn(1)−N(3C)	86.49(9)	N(3B)−Mn(1)−N(3C)	180.0
N(1)−Mn(1)−N(4)	89.20(9)	N(1A)−Mn(1)−N(4)	90.80(9)
N(3B)−Mn(1)−N(4)	88.82(9)	N(3C)−Mn(1)−N(4)	91.18(9)
N(1)−Mn(1)−N(4A)	90.80(9)	N(1A)−Mn(1)−N(4A)	89.20(9)
N(3B)−Mn(1)−N(4A)	91.18(9)	N(3C)−Mn(1)−N(4A)	88.82(9)
N(4)−Mn(1)−N(4A)	180.0	C(1)−N(1)−Mn(1)	155.0(2)
N(1)−C(1)−N(2)	173.5(3)	C(1)−N(2)−C(2)	122.3(3)
N(3)−C(2)−N(2)	171.7(3)	C(2)−N(3)−Mn(1D)	158.8(2)

Results and Discussion

Description of the Crystal Structure of $[Mn(4\text{-bzpy})_2(N(CN)_2)_2]_n$ (1). The labeled diagram for **1** is shown in Figure 1. The structure consists of octahedrally coordinated manganese atoms in which the coordination sites are occupied by two

(7) Escuer, A.; Vicente, R.; Goher, M. A. S.; Mautner, F. A. *Inorg. Chem.* **1998**, *37*, 782.
(8) Walker, N.; Stuart, D. *Acta Crystallogr.* **1983**, *A39*, 158.
(9) Sheldrick, G. M. *SHELXS-86, Program for the Solution of Crystal Structure*; University of Gottingen, Germany, 1986.
(10) Sheldrick, G. M. *SHELXL-93, Program for the Refinement of Crystal Structure*; University of Gottingen, Germany, 1993.
(11) *SHELXTL, Program Library for the Solution and Molecular Graphics, version 5.03 (PC version)*; Siemens Analytical Instruments Division: Madison, WI, 1995.
(12) Spek, A. L. *PLUTON-92*; University of Utrecht: Utrecht, The Netherlands, 1992.

Table 3. Selected Bond Lengths (Å) and Angles (deg) for $[Mn(bpy)(N(CN)_2)_2]_n$ (**2**)

Mn(1)−N(4)	2.187(4)	Mn(1)−N(4A)	2.187(4)
Mn(1)−N(2A)	2.223(4)	Mn(1)−N(2)	2.223(4)
Mn(1)−N(1A)	2.255(3)	Mn(1)−N(1)	2.255(3)
N(2)−C(6)	1.131(5)	C(6)−N(3)	1.275(5)
N(3)−C(7B)	1.295(5)	C(7)−N(4)	1.128(5)
N(4)−Mn(1)−N(4A)	102.1(2)	N(4)−Mn(1)−N(2A)	86.45(14)
N(4A)−Mn(1)−N(2A)	90.72(14)	N(4)−Mn(1)−N(2)	90.72(14)
N(4A)−Mn(1)−N(2)	86.45(14)	N(2A)−Mn(1)−N(2)	175.5(2)
N(4)−Mn(1)−N(1A)	164.35(12)	N(4A)−Mn(1)−N(1A)	93.04(12)
N(2A)−Mn(1)−N(1A)	89.36(13)	N(2)−Mn(1)−N(1A)	94.28(12)
N(4)−Mn(1)−N(1)	93.04(12)	N(4A)−Mn(1)−N(1)	164.35(12)
N(2A)−Mn(1)−N(1)	94.28(12)	N(2)−Mn(1)−N(1)	89.36(13)
N(1A)−Mn(1)−N(1)	72.2(2)	C(6)−N(2)−Mn(1)	158.7(4)
N(2)−C(6)−N(3)	173.2(5)	C(6)−N(3)−C(7B)	120.9(4)
N(4)−C(7)−N(3C)	174.4(5)	C(7)−N(4)−Mn(1)	161.9(4)

N-pyridine atoms of two 4-benzoylpyridine ligands in trans arrangement and four N-terminal atoms of dicyanamide ligands. Two of the dicyanamide ligands act as end-to-end bridging ligands with one neighboring manganese atom, and the other two also act as end-to-end bridging ligand with the other neighboring manganese atom, giving a uniform one-dimensional system (Figure 1). The bond parameters related to the bridges are Mn(1)−N(1) = 2.212(2) Å, Mn(1)−N(3B) = 2.221(3) Å, Mn(1)−N(1)−C(1) = 155.0(2)°, and Mn(1)−N(3B)−C(2B) = 158.8(2)°. The dicyanamide ligand is angular with a C(1)−N(2)−C(2) angle of 122.3(3)° with two nearly linear N−C−N units with angles of 173.5(3)° and 171.7(3)°. The shortest intrachain Mn−Mn distance is 7.584(2) Å (*b* axis of the cell) as consequence of the large bridging ligand, whereas the minimum interchain Mn−Mn is only 6.374(2) Å (*a* axis of the cell). Along the *c* direction the minimum Mn−Mn distance is 14.172(2) Å (Figure 2). The $Mn(NCNCN)_2Mn$ ring shows a slight chair distortion from planarity, with a maximum deviation of the manganese atoms of 0.212 Å over the plane defined by the two dicyanamide ligands (angle between the mean plane of the dicyanamide ligands and the N(1)−Mn(1)−N(3D) plane is 8.0(1)°).

Description of the Crystal Structure of *cis*-$[Mn(bpy)(N(CN)_2)_2]_n$. The labeled diagram for **2** is shown in Figure 3. This compound has the same double dicyanamide bridges in a one-dimensional arrangement, similar to the above compound with 4-bzpy, but the chelate character of 2,2′-bpy leads to the cis 1D compound. The bond parameters of the bridging region are also quite similar to those of **1**: Mn(1)−N(2) = 2.223(4) Å, Mn(1)−N(4) = 2.187(4) Å, Mn(1)−N(2)−C(6) = 158.7(4)°, and Mn(1)−N(4)−C(7) = 161.9(4)°. The dicyanamide ligand is bent with a C(6)−N(3)−C(7B) angle of 120.9(4)° and two N−C−N straight linear units with angles of 173.2(5)° and 174.4(5)° for N(2)−C(6)−N(3) and N(4)−C(7)−N(3C), respectively.

The shortest intrachain Mn−Mn distance is 7.512(3) Å (*b* axis of the cell) as consequence of the large bridging ligand, whereas the minimum interchain Mn−Mn is 6.707(3) Å with neighboring chains in the (100) direction (Figure 2). In this case the $Mn(NCNCN)_2Mn$ rings are roughly planar, with deviation from the mean plane of less than 0.1 Å for all atoms.

Magnetic Data and Coupling Constants Evaluation. The $\chi_M T$ product and the molar magnetic susceptibilities vs T in the 300−2 K range of temperature for $[Mn(4\text{-bzpy})_2(N(CN)_2)_2]_n$ (**1**) and $[Mn(bpy)(N(CN)_2)_2]_n$ (**2**) are plotted in Figure 4. The overall behavior of **1** and **2** corresponds to weak antiferromagnetically coupled systems. When the samples are cooled, the $\chi_M T$ product decreases slowly from 4.20 and 4.36 $cm^3\ K\ mol^{-1}$ at 300 K for **1** and **2**, respectively, decreases more quickly below 50 K, and tends to zero at low temperature. The χ_M value increases continuously on cooling. The magnetic data were analyzed by means of the analytical expression[13] for an infinite chain of classical spins derived by Fisher:

$$\chi = \left[\frac{Ng^2\beta^2S(S+1)}{3kT}\right]\left[\frac{1+u}{1-u}\right]$$

with

$$u = \coth\left[\frac{JS(S+1)}{kT}\right] - \frac{kT}{JS(S+1)}$$

Best-fit parameters were $J = -0.3\ cm^{-1}$, $g = 1.98$; $J = -0.4\ cm^{-1}$, $g = 2.00$ for **1** and **2**, respectively. The weak antiferromagnetic interaction was confirmed by magnetization measurements at 2 K up to an external field of 5 T. At higher field, the magnetization in M/Nβ units indicates a quasi-saturated $S = {}^5/_2$ system for both compounds (Figure 5). Comparison of the overall shape of the plots with the Brillouin plot for a fully isolated $S = {}^5/_2$ system indicates slower magnetization consistent with a weak AF interaction. These low J values compare well with the weak coupling found for the few examples of dicyanamide or tricyanomethanide compounds measured to date.

EPR spectra recorded on powdered samples at room temperature show an isotropic signal centered at $g = 2.00$, with a peak-to-peak line width of 90 G for **1** and 121 G for **2**. In addition, a weak half-field signal centered at $g = 4.00$ was found for both complexes. The $g = 2.00$ signal shows the same line width at 77 K, increasing slightly at 4 K ($\Delta H_{pp} = 200$ G). The room-temperature line width is between those of the sharp signals ($\Delta H_{pp} = 35$ G at room temperature) recently reported for the structurally related compounds with end-to-end azide bridges,[7,14] $[Mn(pyOH)_2(\mu\text{-}N_3)_2]_n$, $[Mn(3\text{-}etpy)_2(\mu\text{-}N_3)_2]_n$, and $[Mn(3,5lutidine)_2(N_3)_2]$, and those of the very broad signal ($\Delta H_{pp} = 750$ G) reported for the end-on azide-bridged system $[Mn(2\text{-}bzpy)(N_3)_2]_n$ (2-bzpy = 2-benzoylpyridine).[14]

This behavior may be explained by attending to the main factors[15] that influence the line width for an isotropic Heisenberg one-dimensional system: exchange narrowing, due to the superexchange interactions along the chain, and intra- or interchain dipolar interactions that broaden the signal. For the two $[Mn(L)_2(\mu\text{-}N_3)_2]_n$ complexes, the chains were neutral and well isolated by the large pyridinic ligands (Mn···Mn interchain distance greater than 9 Å) and the intrachain Mn···Mn distances were around 5.3 Å.[7] From these structural parameters, dipolar intra- or interchain interactions are negligible, and so the narrower signals observed for the azido chains may be attributed to the exchange narrowing: very weak for **1** and **2** ($|J| < 0.5\ cm^{-1}$) and strong for the two $[Mn(L)_2(\mu\text{-}N_3)_2]_n$ compounds ($|J|$ values close to 10 cm^{-1}). In contrast, dipolar interactions explain the large line width found in the EPR signal (750 G) of the end-on azide-bridged chain $[Mn(2\text{-}bzpy)(N_3)_2]_n$, which shows comparable J superexchange parameters ($J = 0.8\ cm^{-1}$) and interchain Mn···Mn distances but strong dipolar interactions due to the short Mn···Mn intrachain distances,[14] close to 3.5 Å.

Superexchange Mechanism. A priori, weak interactions may be expected for the end-to-end dicyanamide bridges, present because of the large Mn−Mn interaction pathway through a

(13) Fisher, M. E. *Am. J. Phys.* **1964**, *32*, 343.
(14) Abu-Youssef, M. A. M.; Escuer, A.; Gatteschi, D.; Goher, M. A. S.; Mautner, F. M.; Vicente, R. *Inorg. Chem.* **1999**, *38*, 5716.
(15) Bencini, A.; Gatteschi, D. *EPR of Exchange Coupled Systems*; Springer-Verlag: Berlin, Heidelberg, 1990; Chapter 10 and references therein.

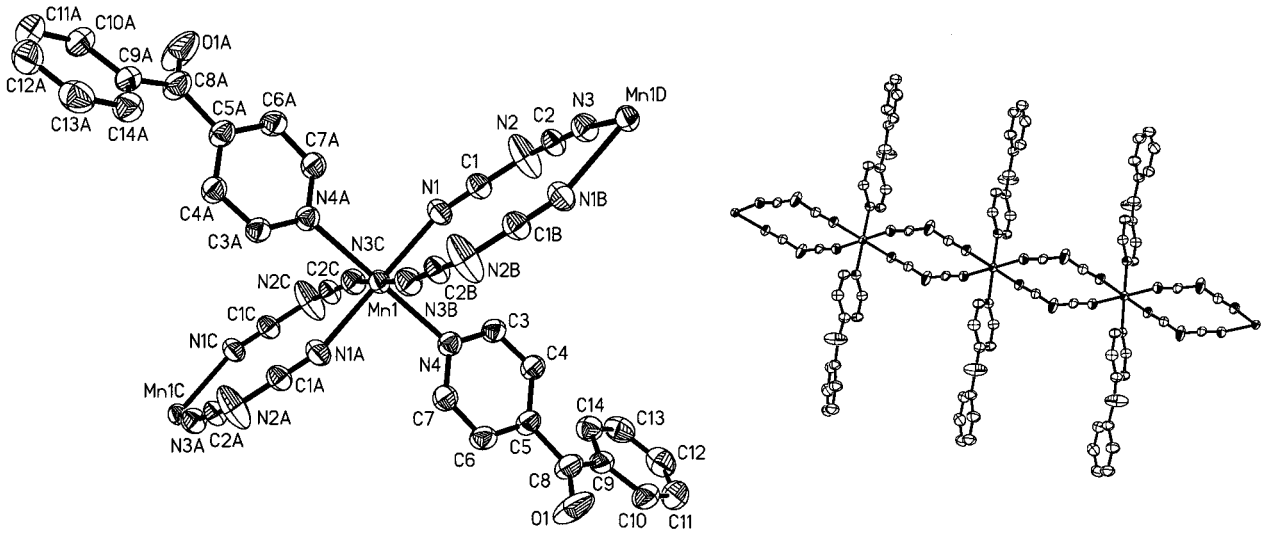

Figure 1. Labeled ORTEP drawing for *trans*-$[Mn(4\text{-bzpy})_2(N(CN)_2)_2]_n$ (**1**). Ellipsoids are shown at the 40% probability level together with a view of the chain arrangement.

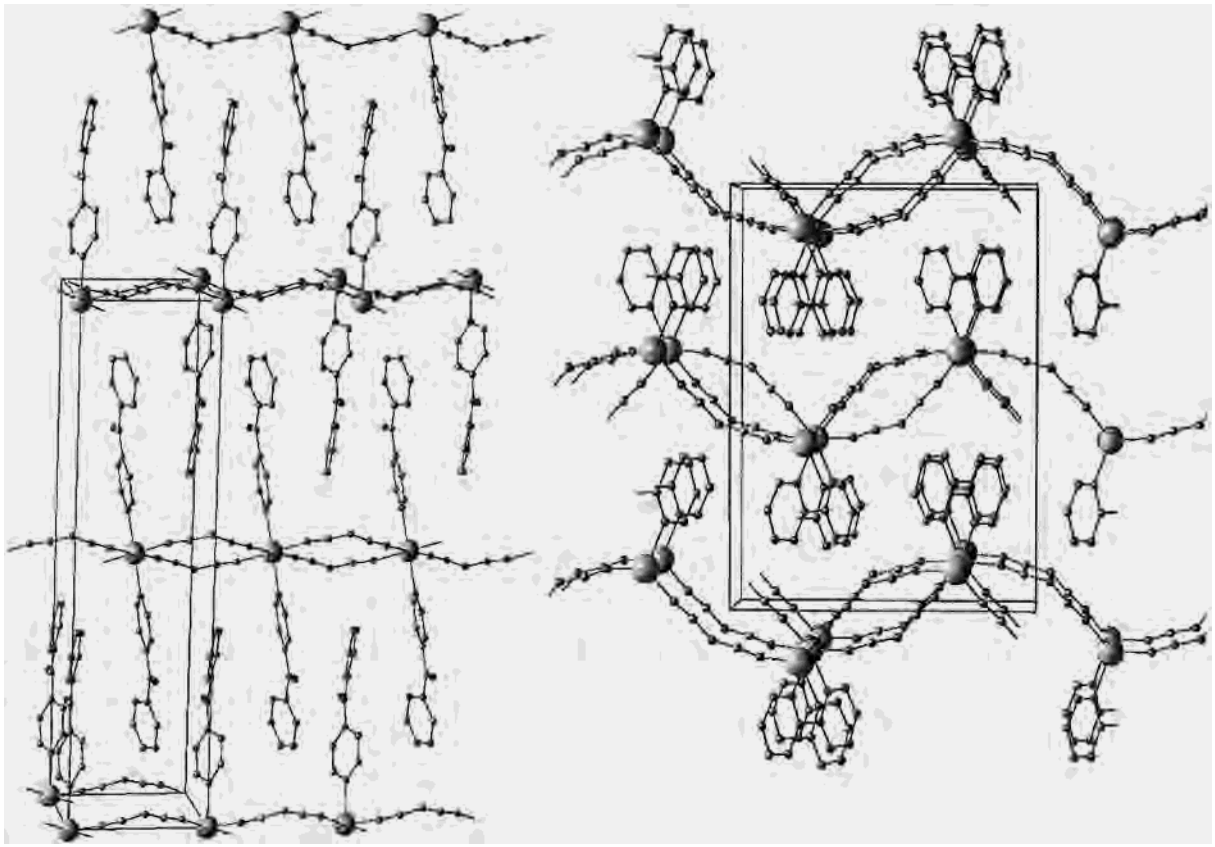

Figure 2. View along (001) direction of the unit cell of *trans*-$[Mn(4\text{-bzpy})_2(N(CN)_2)_2]_n$ (**1**) and *cis*-$[Mn(bpy)(N(CN)_2)_2]_n$ (**2**) compounds showing the packing of the chains.

bridge of five atoms. This is important, but it is not the only factor that promotes very weak coupling between the paramagnetic centers. MO calculations[16] performed on the dicyanamide ligand and also on a modeled dimeric unit show some determinant topological factors that may be compared with the very effective end-to-end azide bridge. The model used for the calculation was a $[(NH_3)_4Mn-(\mu_{1,5}\text{-dca})_2-Mn(NH_3)_4]^{2+}$ unit with the bond parameters Mn−N 2.150 Å, N−C 1.130 and 1.290 Å, Mn−N−C 164.0°, N−C−N 180°, and C−N−C 122.0°.

The main superexchange pathways for the azide ligand consist of two degenerate π_x and π_y nonbonding MOs that may overlap with the appropriate atomic orbitals of the paramagnetic center.[17] For the angular dicyanamide ligand, the two HOMOs correspond to one π nonbonding and one σ orbital, not strictly degenerate but with similar energy. For both azide and dicyanamide ligands, one of the HOMOs of the bridge corresponds to one π

(16) Mealli, C.; Proserpio, D. M. CACAO program (Computed Aided Composition of Atomic Orbitals). *J. Chem. Educ.* **1990**, *67*, 399.

(17) Kahn, O. *Molecular Magnetism*; VCH Publishers: New York, 1993 and references therein.

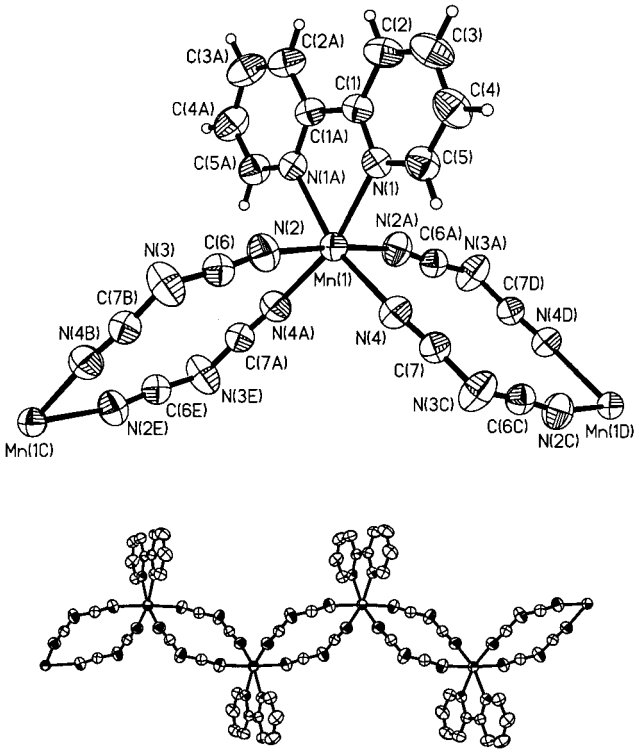

Figure 3. Labeled ORTEP drawing for *cis*-$[Mn(bpy)(N(CN)_2)_2]_n$ (**2**). Ellipsoids are at 30% probability level, and a view of the chain arrangement is shown.

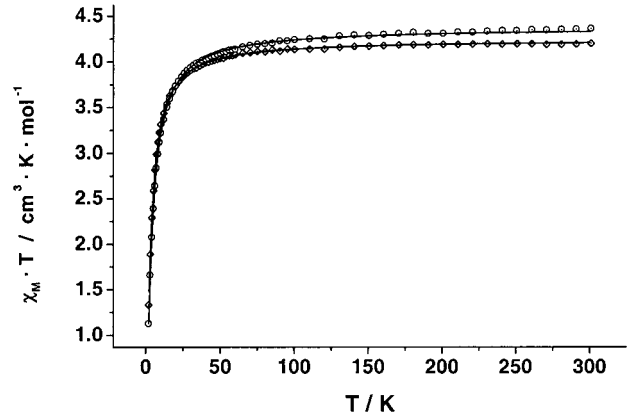

Figure 4. Plot of the $\chi_M T$ product vs T for compounds *trans*-$[Mn(4\text{-}bzpy)_2(N(CN)_2)_2]_n$ (**1**) (dot-centered diamonds) and *cis*-$[Mn(bpy)(N(CN)_2)_2]_n$ (**2**) (dot-centered circles). Solid line shows the best fit of the data (see text).

Chart 2

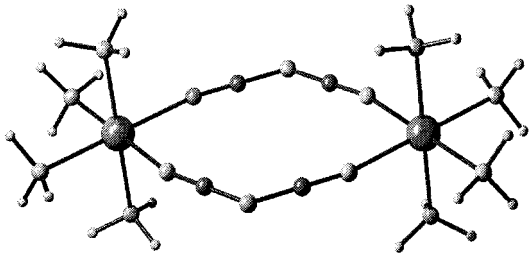

nonbonding orbital (Figure 6) with a similar difference in energy with the d orbitals of the metal. These π MOs may overlap appropriately with the corresponding t_{2g} atomic orbitals of a paramagnetic center such as Mn(II) (d^5 ion). The poor efficiency of this pathway compared with the π nonbonding orbital of the

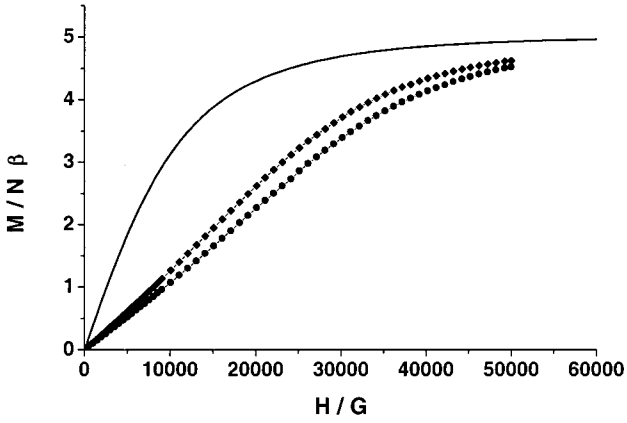

Figure 5. Plot of the magnetization in 2S units measured at 2 K for the compounds *trans*-$[Mn(4\text{-}bzpy)_2(N(CN)_2)_2]_n$ (**1**) (solid diamonds) and *cis*-$[Mn(bpy)(N(CN)_2)_2]_n$ (**2**) (solid circles). Continuous line corresponds to the Brillouin function for an isolated $S = {}^5/_2$. Lower magnetization for **2** confirms a J value slightly greater than that of compound **1**.

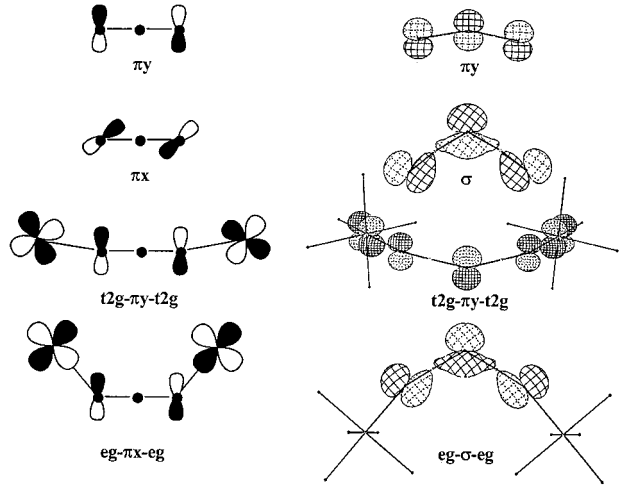

Figure 6. Left: schematic drawing of the main superexchange pathways for the azido ligand. Right: the corresponding π_y and σ MOs for the dicyanamide ligand together the schematic superexchange pathways. The efficiency of the $t_{2g}-\pi_y-t_{2g}$ interaction is reduced for the dicyanamide ligand because of the lower density of the bridge on the terminal N atoms (25% vs 50% for the azido bridge). For the $e_g-\sigma-e_g$ interaction, the N−Mn bond direction is close to the nodal plane, giving a negligible net overlap, in contrast with the very efficient $e_g-\pi_x-e_g$ interaction found for the azido bridge.

azido system lies in the lower electronic density on the terminal N atoms. For the N_3^- ion the electronic probability on the terminal N atoms is 50%, whereas for the dicyanamide ligand the maximum of probability resides on the central nitrogen and only 25% lies on the terminal N atoms. Consequently, the overlap is drastically reduced, and this superexchange pathway thus becomes less efficient for the dicyanamide ligand than the azide bridge.

For the azido bridge, the most effective pathway that gives strong antiferromagnetism for moderate or medium M−N−N bond angles is the second π orbital, which may interact with the e_g orbitals of the paramagnetic centers, giving an $e_g-\pi-e_g$ pathway with good overlap.[7,17] For the dicyanamide ligand, the equivalent pathway consists of an $e_g-\sigma-e_g$ interaction, which, for the experimental M−N−C bond angles in all cases close to 160°, shows a net overlap close to zero, as may be observed in the Figure 6 in addition to the lower density in the terminal N atoms.

The immediate conclusion is that the $\mu_{1,5}$-dicyanamide bridge should be assumed to be a very poor superexchange mediator, and practically noncoupled systems should be expected. The above conclusions can be easily extrapolated to the $\mu_{1,3}-\mu_{3,5}$ bridges recently found in the $[M(dca)_2]$ compounds; the σ pathway for M−N−C bond angles close to 160° should always allow reduced overlap and low magnetic interaction, and the main (and experimentally low[1−3]) interactions may be related to the moderately effective π pathway. The most important consequence of these results is the predictable low interaction for all coordination modes of the dicyanamide bridge, which should lead to low T_c in extended systems.[18]

Acknowledgment. A. Escuer and R. Vicente thank the CICYT (Grant PB96/0163) for support of this research. F. A. Mautner thanks Prof. C. Kratky and Prof. F. Belaj (University of Graz) for use of experimental equipment and the OENB for partial financial support (Project 7967).

Supporting Information Available: A complete listing of data collection and processing parameters, bond lengths and bond angles, atomic coordinates, anisotropic displacement coefficients, and hydrogen atom coordinates for **1** and **2**. This material is available free of charge via the Internet at http://pubs.acs.org.

IC990905H

(18) During the refereeing process of this paper, some related chains have been reported by other authors, showing always very low coupling constants. Manson, J. L.; Arif, A. M.; Miller, J. S. *J. Mater. Chem.* **1999**, *9*, 979. Batten, S. R.; Jensen, P.; Kepert, C. J.; Kurmoo, M.; Moubaraki, B.; Murray, K. S.; Price, D. J. *J. Chem. Soc., Dalton Trans.* **1999**, 2987. Manson, J. L.; Arif, A. M.; Incarvito, C. D.; Liable-Sands, L. M.; Rheingold, A. L.; Miller, J. S. *J. Solid State Chem.* **1999**, *145*, 369.